EPJ manuscript No.
(will be inserted by the editor)

Angular dependence of double electron capture in collisions of C^{4+} with He

Stueckelberg oscillations in the differential cross section for capture into $C^{2+}(1s^2 2s^2\ ^1S)$

Lukáš Pichl[1a], Reiko Suzuki[2], Mineo Kimura[3], Yan Li[4], Robert J. Buenker[4], Masamitsu Hoshino[5], and Yasunori Yamazaki[6]

[1] Max Planck Institute for the Physics of Complex Systems, Nöthnitzer Str. 38, D01187 Dresden, Germany
[2] Computer Center, Hitotsubashi University, Kunitachi, Tokyo 186-8601, Japan
[3] Graduate School of Sciences, Kyushu University, Fukuoka 812-8581, Japan
[4] Fachbereich C-Mathematik und Naturwissenschaften, Bergische Universität Wuppertal, D-42119 Wuppertal, Germany
[5] Department of Physics, Sophia University, 7-1 Kioicho, Tokyo 102-8554, Japan
[6] RIKEN, 2-1 Hirosawa, Wako 351-0198, Japan

Received: July 30th, 2005 / Revised version:

Abstract. In charge-transfer collisions of $C^{4+}(1s^2\ ^1S)$ with He $(1s^2\ ^1S)$, the process of double electron capture into the ground state C^{2+} is well known to dominate other channels by an order of magnitude for projectile energies below 10 keV. This work presents a calculation of differential cross-sections resolved in the angle and energy gain variables, based on an ab initio treatment of electronic states, and compares with the measurements published in the literature (projectile energy E=270, 400, and 470 eV). We also briefly discuss the semi-empirical two-state models developed by experimentalists for this process.

PACS. 34.70.+e charge transfer – 31.15.Ar ab initio calculations

1 Introduction

Experimental data on electron capture in charge transfer collisions of C^{4+} with He have been abundant in the literature, both for integral and angle-differential cross sections [1–5]. By contrast, theoretical works based on ab initio potentials are extremely scarce; this is in part due to the difficulty in calculating the interaction between the closed $1s^2$ shells of C^{4+} projectile and He target, the polarization term. The most elaborate theoretical work to date presents a calculation of integral single-capture (SC) and double-capture (DC) cross sections by Kimura and Olson [6], who used an ion-core pseudo-potential for $C^{2+}(1s^2)$, dealing explicitly with the two active valence electrons. Ref. [6] provides the integral cross section data for projectile energies between 750 eV and 200 keV.

To date, experimentalists have mostly relied upon semi-empirical representations of the system (e.g. 2-state model in Ref. [3] or 4-state model in Ref. [4]), using polarization and Coulomb type diabatic potentials with position-dependent effective charges, or potentials defined as an interpolation between the asymptotic terms for low and large internuclear distance R. In either case, the coupling between the diabatic states was estimated by an elaborate analytical formula of Grozdanov and Janev [7] with adjusted parameters. Model potential curves were also used to deduce the diabatic coupling in an inverse problem (fitting model to cross section data) [8], resulting in different coupling terms than in Ref. [7]. By using free parameters in the model formulas, experimental data could be modelled rather accurately, yet the potentials and coupling terms vary among the experimental groups. Clearly, since CHe^{+4} is now an inexpensive 4-electron system even for large basis sets, a full ab initio calculation is therefore preferable. The differential cross-sections also depend more strongly on the details of the interaction, and represent a stricter test on the accuracy of theory as compared to the integral cross sections published before [6].

Here we calculate the differential cross-sections for the above process, motivated by recent publications of state-resolved angle-differential and energy-gain differential cross sections in the literature [1,2]. The differential cross-sections for the main capture channel are evaluated in both equivalent forms, and compared with the experimental data available for the collision energy E=270, 400 and 470 eV.

The paper is organized as follows. Section 2 summarizes the ab initio calculation and compares the resulting potentials and couplings to empirical models used by experimentalists. Section 3 briefly explains the standard theoretical procedure and lists the kinematic and cross-

Send offprint requests to: lukas@pichl.jp
[a] *On summer leave from:* International Christian University, Osawa 3-10-2, Mitaka, Tokyo 181-8585, Japan

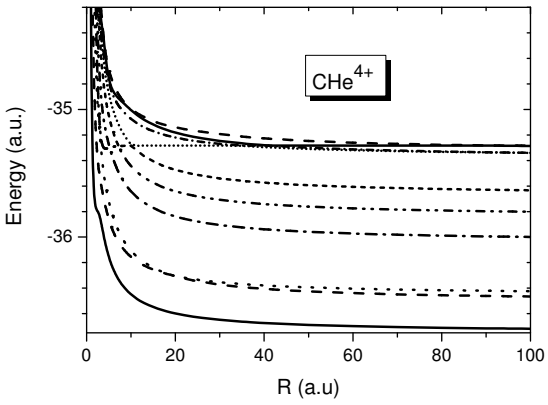

Fig. 1. Potential energy curves of CHe^{4+}: asymptotic region

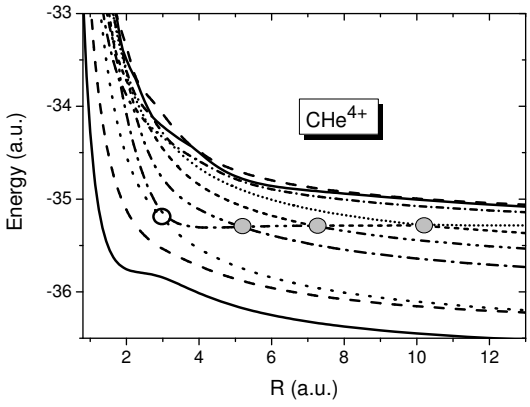

Fig. 2. Potential energy curves of CHe^{4+}: transition region

section transform relations in order to compare with the experiment. Results are discussed in Section 4. Section 5 concludes the paper. Atomic units are used throughout unless mentioned otherwise.

2 Electronic States of CHe^{4+}

In order to obtain the potential curves of the C^{4+}/He system, we have carried out ab initio configuration interaction calculations by using an extended version of the multireference single- and double excitation MRD-CI programs [9]. The correlation consistent polarized valance quadruple zeta, cc-pVQZ Gaussian basis [10] was employed for the C and He atoms. A selection threshold of 10^{-9} Hartree was used to select the configuration wave functions of which the electronic wave functions are composed. Nonadiabatic couplings $< Q(R)_i|\mathrm{d}Q(R)_j/\mathrm{d}R >$ were evaluated by using a numerical differentiation method. The lowest 13 electronic states of $^1A_1$ symmetry (12 Σ states and a Δ state) were tracked for internuclear distances ranging between 0.8 and 100 au. In solving the coupled equations, three highly excited states in the loosely coupled manifold were dropped because of their negligible coupling to the initial state and sensitivity to configurations below the selection threshold.

Figure 1 shows the manifold of electronic state potential energy curves for the ten electronic states considered in the calculation. The initial channel is flat as the polarization terms behaves $\sim R^{-4}$. The potential in capture channels decays as $3/R$ (SC) or $4/R$ (DC). At $R = 100$, the state assignment is as follows (numbering with increasing energy): 1, 3, and 8 are single capture states; 2, 4, 5-9 are double-capture states; the initial state is No. 10; all capture is driven by the behavior of electronic states and their nonadiabatic coupling (both radial and angular components) at shorter distances, where exothermic transitions may take place. The location of avoided crossings along the $1s^2$-$1s^2$ curve is shown in Fig. 2; grey circles show a sequence of diabatic crossings, while the empty

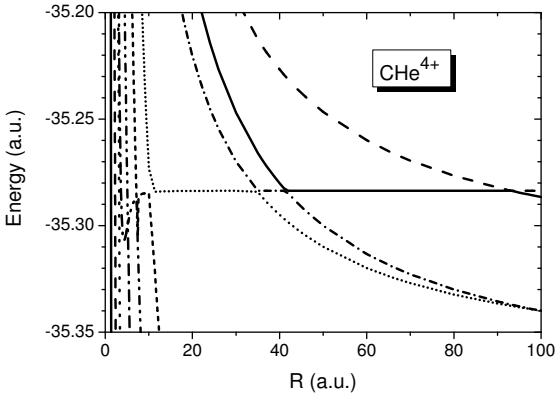

Fig. 3. Initial channel $C^{4+}(1s^2\ ^1S)$ - $He(1s^2\ ^1S)$ (flat line)

circle indicates the key crossing point responsible for double electron capture to the He^{2+} ground state. The grey circles practically mean a mere change of electronic state label, since the electronic potential curves almost touch; also the electronic wave functions show that the electronic configurations are conserved along the crossing lines. Detailed behavior of the potential curve corresponding to the initial channel and its diabatic crossings can be seen in Fig. 3.

The values of nonadiabatic couplings for R above the potential ridge $R \sim 2$ clearly indicate that the avoided crossing in Fig. 3 ($R_x \sim 3$) is by far the main transition mechanism, in accordance with previous findings [4]. All other crossings of the initial state above the ridge are largely diabatic. At the transition region, the FWHM of the broad coupling peak is $R_{FWHM} \sim 0.38$ a.u., and throughout this region the two potential energy curves go in parallel. This can be seen in Fig. 4 in more detail, along with the empirical potential curves used by Danared and Barany in analytical form [3] (dashed line). The crossing point calculated here is 0.5 a.u. lower than that of the model potentials (dashed line) [3]. The adiabatic curves

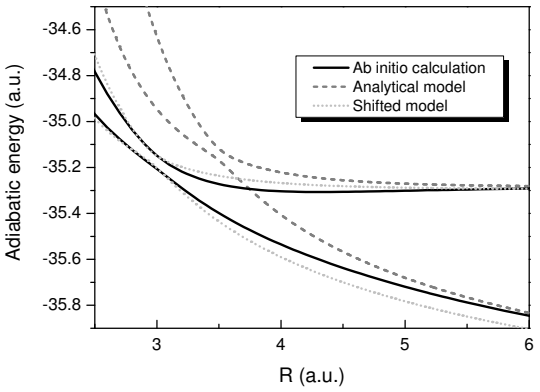

Fig. 4. Adiabatic curves: two-state model

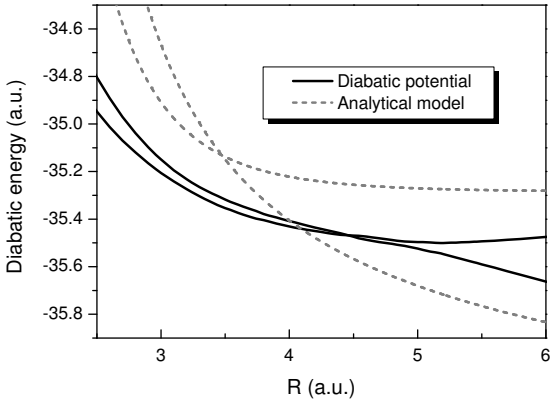

Fig. 5. Diabatic curves: two-state model

from our calculation coincide well with the model potentials shifted to the transition point (dotted line) throughout the entire transition region, but differ at larger distances. Such a difference should not have an impact on the transition probabilities, although it may appear as a phase in the scattering amplitudes.

Figures 5 shows the diabatic potentials, which are obtained by a rotation matrix $\underline{C}$ applied on the 2-by-2 diagonal matrix of adiabatic potentials. The matrix $\underline{C}$ satisfies

$$\underline{C}(R) = \underline{I} + \int_R^\infty \underline{A}(R')\underline{C}(R')\mathrm{d}R', \qquad (1)$$

where $A_{i,j}(R) = (1-\delta_{i,1-j})\langle i|\mathrm{d}/\mathrm{d}R|j\rangle$ for $i,j = 1,2$. In the basis of electronic states rotated by $\underline{C}(R)$, all nonadiabatic coupling terms identically vanish. Such an representation is required in the full quantum calculations [11, 12]. The present results differ quite significantly from the shifted model diabatic potentials. This is plausible since in general, the adiabatic potential matrix includes only the two eigenvalues, while a full 2-by-2 hamiltonian matrix consists of three independent elements, and its details depend on the behavior of the derivative coupling term.

3 Charge Transfer Collision Dynamics

In this section, we review the standard kinematic relations and reference frame transforms [13], and summarize the procedure to obtain differential cross sections.

The angle-differential cross section in the laboratory system (angle θ_L) consists of two contributions in the center-of-mass frame, $\theta_{CMS\pm} =$

$$\cos^{-1}\left[-\xi\sin^2\theta_L \pm (1-\xi^2\sin^2\theta_L)^{1/2}\cos\theta_L\right], \qquad (2)$$

with $\xi = m_1 v_i/(m_2 v_f)$, where $m_{1,2}$ is the mass of the projectile and the target, respectively, and $v_{i,f}$ the initial and final relative velocity. The differential cross sections then transform as

$$\frac{\mathrm{d}\sigma}{\mathrm{d}\Omega_L}(\theta_L) = \frac{\left(1+2\xi\cos\theta_L+\xi^2\right)^{3/2}}{|1+\xi\cos\theta_L|}\frac{\mathrm{d}\sigma}{\mathrm{d}\Omega_{CMS}}(\theta_{CMS}), \quad (3)$$

for scattering angles up to the maximum $\theta_{L,max} = \sin^{-1}\xi^{-1}$.

Given a particular gain/loss of projectile internal energy Q in the scattering event, the energy gain of the projectile (energy E_0) and the scattering angle are equivalent, according to

$$\Delta(E) = \left(\frac{m_1}{m_1+m_2}\right)^2 E_0\cos^2\theta_L\,\{1+[1- \\ -\frac{m_2^2+m_1m_2}{m_1^2\cos^2\theta_L}\left(\frac{m_1}{m_2}-1-\frac{Q}{E_0}\right)\Big]^{1/2}\Big\}^2 - E_0, \qquad (4)$$

which yields the cross-section transform

$$-\frac{\mathrm{d}\sigma}{\mathrm{d}(\Delta E)} = \\ \frac{\pi(m_1+m_2)^2(1+\gamma/\cos^2\theta_L)^{1/2}}{m_1^2E_0\cos\theta_L[1+(1+\gamma/cos^2\theta_L)^{1/2}]^2}\frac{\mathrm{d}\sigma}{\mathrm{d}\Omega_L(\theta_L)}. \qquad (5)$$

The de Broglie wave length of the projectile at the lowest energy considered in this work is 1.5×10^{-3} a.u., due to the large mass of the C^{4+} projectile, and much below the characteristic distance of the potential matrix. Therefore we apply the eikonal approximation to solving the coupled equations for state-dependent amplitudes $c_{j,i_0}(b,z)$, j=1, 10. The semiclassical formulation of these equations is given in detail in Refs. [14,15] (cf. also references therein) and thus will not be repeated here. The cross-section then follows from the diffraction integral,

$$\frac{\mathrm{d}\sigma}{\mathrm{d}\Omega}(\theta) = (mv)^2\left|\int_0^\infty J_0(\eta b)c_{fi_0}(b;\infty)b\mathrm{d}b\right|^2, \qquad (6)$$

where m is the reduced mass, v is the relative collision velocity, J_0 is the Bessel function and $\eta = 2mv\sin(\theta/2)$ [14]. To calculate the diffraction integral in Eq. (6), we employ a 10,000-point grid of impact parameters.

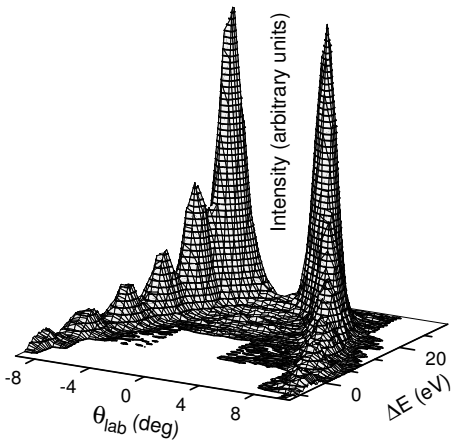

Fig. 6. Double-differential cross section for double electron capture to $C^{2+}(1s^2 2s^2\ ^1S)$

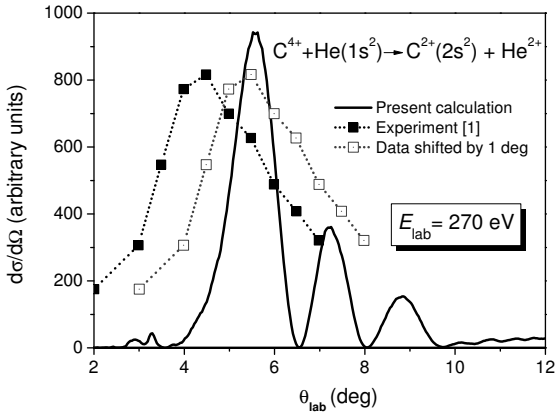

Fig. 7. Angle-differential cross section for electron double capture to $C^{2+}(1s^2 2s^2\ ^1S)$ at 270 eV

4 Results and Discussion

Before presenting the calculated cross section results, let us briefly discuss the experimental results previously published [2]. Figure 6 shows a map of the differential cross section at E_0=400 eV resolved both in the angle θ_L and energy gain/loss $\Delta(E)$ variables. The parabolic border along which the cross-section peaks are located is given by Eq. (4) with Q ∼33.4 eV, which corresponds to the transition from C^{4+} ground-state to C^{2+} ground state. In the following, we compare theoretical data to the measurements by Hoshino et al. published previously [1,2].

The angle differential cross sections calculated for E_0 = 270, 400 and 470 eV are shown in Figs. 7, 8 and 9 (full lines), along with the experimental values arbitrarily scaled in the vertical direction (full squares). It can be seen that the previous experiments could not resolve well oscillatory structures in the θ_L dimension. In Figs. 7 and 9, we apply small horizontal shifts of experimental data to the left, which is within the experimental error bars [1,2]. Next, the situation substantially improves when we compare with the differential cross sections resolved in the energy gain/loss variable ΔE, i.e. the two-dimensional map in Fig. 6 integrated over the θ_{lab} variable. Since the experimental cross sections are subject to much smaller errors in $\Delta(E)$, the oscillatory cross section structures in Fig. 10 are now much better resolved. The agreement of the present results with experiment in Fig. 10 is considered to be very good, especially when taking into account the sensitivity of differential cross sections to the details of ab initio potentials and couplings.

The calculated angle-differential cross-sections in Figs. 7-9 clearly show the existence of Stueckelberg oscillations. Due to relatively weak coupling of other channels, the cross section minima fall near zero, which is a typical feature for two-state systems. Therefore in order to asses the applicability of two-state classical models to the present results, we have also calculated the semiclassical phases

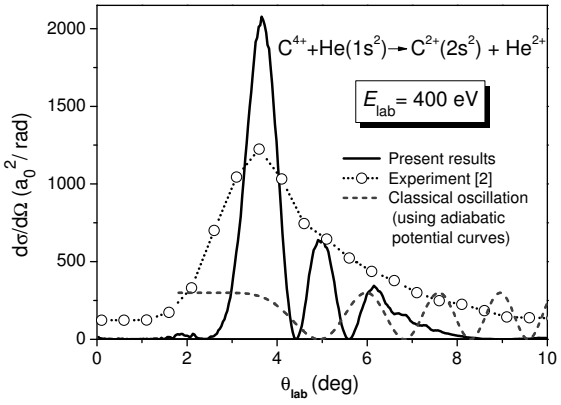

Fig. 8. Angle-differential cross section for electron double capture to $C^{2+}(1s^2 2s^2\ ^1S)$ at 400 eV

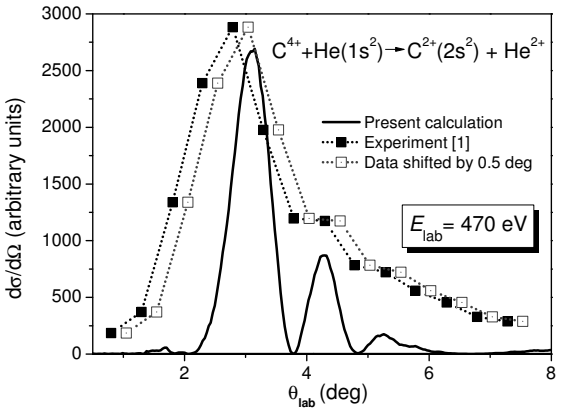

Fig. 9. Angle-differential cross section for electron double capture to $C^{2+}(1s^2 2s^2\ ^1S)$ at 470 eV

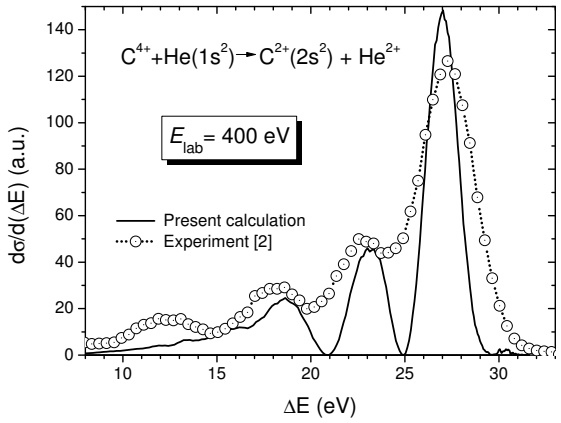

Fig. 10. Energy-gain differential cross section for double electron capture to $C^{2+}(1s^2 2s^2\ ^1S)$ at 400 eV

on the ab-initio adiabatic potentials, i.e. $\theta_{CMS,i}(b) =$

$$\pi - 2b \int_{R_{t,i}}^{R_x} \frac{\mathrm{d}R}{R^2(1 - U_i(R)/E - b^2/R^2)^{1/2}}, \qquad (7)$$

$i = 1, 2$. Here $R_{t,i}$ is the turning point on adiabatic potential U_i and R_x the crossing point. The Stueckelberg phase in the semiclassical model is then given by the phase integral of the inverse function along the two $b_i(\theta)$ branches [3],

$$\phi(\theta_{CMS}) = \sqrt{2mE} \int_{\theta(R_x)}^{\theta_{CMS}} (b_1(\theta) - b_2(\theta))\mathrm{d}\theta \qquad (8)$$

The oscillatory factor $\cos(\phi(\theta_{lab}))$ is shown in Fig. 8 as a dashed line. It can be inferred that the classical picture alone does not apply to the present case, which is especially due to (1) delocalized transition in the broad vicinity of the crossing point, and (2) neglect of transition phases at the crossing point.

5 Concluding Remarks

We have calculated the differential cross sections for double electron capture to C^{2+} ground-state in the collisions of C^{4+} with He based on ab initio potentials and couplings. The double electron capture channel to $C^{2+}(1s^2 2s^2\ ^1S)$ by far dominates the other states, which could be explained by the analysis of the crossing point in the delocalized transition region. The present diabatic potential matrices and double capture cross sections differ from those based on the 2-state model [3]; the adiabatic potentials agree well up to a horizontal shift. The Stueckelberg oscillations in the calculated results could not be resolved in the data measured by Hoshino et al [1,2] because of insufficient resolution in the experiment. On the other hand, the oscillatory structures in the energy gain differential cross sections agree very well with the experimental data, suggesting this kind of spectroscopy to be a useful tool for studying state-resolved electron capture processes. Further experimental work is in progress to confirm the cross section structures seen in the theoretical calculation.

Acknowledgements

This work was supported in part by the Japan Society for the Promotion of Science (JSPS), the Japanese Ministry of Science, Sports, Culture and Education (MEXT), and by the grant BU 450/7-3 of the Deutsche Forschungsgemeinschaft and the Fonds der Chemischen Industrie. L. Pichl acknowledges support by a JSPS Grant-in-Aid, Max Planck Society, and the Academic Frontier Program by MEXT. Special thanks are due to Prof. T. Kasai.

References

1. M. Hoshino, M. Kitajima, Y. Kanai, Y. Nakai, H. Tanaka, and Y. Yamazaki, Physica Scripta T **92**, (2001) 339-340.
2. M. Hoshino, Y. Kanai, F. Mallet, Y. Nakai, M. Kitajima, H. Tanaka, and Y. Yamazaki, Nuclear Instruments and Methods in Physics Research B **205**, (2003) 568-572.
3. H. Danared and A. Barany, J. Phys. B: At. Mol. Phys. **19**, (1986) 3109-3120.
4. M. Barat, P. Roncin, L. Guillemot, M. N. Gaboriaud, and H. Laurent, J. Phys. B: At. Mol. Phys. **23**, (1990) 2811-2818.
5. N. Keller, L. R. Andersson, R. D. Miller, M. Westerlind, S. B. Elston, I. A. Sellin, C. Biedermann, and H. Cederquist, Phys. Rev. A **48**, (1993) 3684-3688.
6. M. Kimura and R. E. Olson, J. Phys. B: At. Mol. Phys. **17**, (1984) L713-L719.
7. T. P. Grozdanov and R. K. Janev, J. Phys. B: At. Mol. Phys. **13**, (1980) 3431-3442.
8. R. Bloyd, T.-S. Ho, and H. Rabitz, J. Chem. Phys. **106**, (1997) 6548-6551.
9. R. J. Buenker, and S. D. Peyerimhoff, Theo. Chim. Acta **35**, (1974) 33; **39**, 217 (1975); R. J. Buenker, Int. J. Quantum Chem. **29**, (1986) 435; S. Krebs, and R. J. Buenker, J. Chem. Phys. **103**, (1995) 5613.
10. T. H. Dunning, Jr., J. Chem. Phys. **90**, (1989) 1007-1023.
11. T. G. Heil, S. E. Butler, A. Dalgarno, Phys. Rev. A. **23**, (1981) 1100-1109.
12. L. B. Zhao, P. C. Stancil, H. P. Liebermann, P. Funke, and R. J. Buenker, Phys. Rev. A **71**, (2005) 060701:1-4.
13. T. G. Heil and J. B. Sharma, Phys. Rev. A **36**,(1987) 3669-3673.
14. W. Fritsch and C. D. Lin, Phys. Rev. A **54**, (1996) 4931-4942.
15. M. Kimura and N. F. Lane, Adv. At. Mol. Opt. Phys. **26**, (1989) 79.